Regional stress in a noncircular cylinder

Ronald F. Janz, Siddik Ozpetek,* Leonard E. Ginzton,‡ and Michael M. Laks
*Edwards LIS Division, Baxter Healthcare Corporation, Irvine, California 92714; ‡Division of Cardiology, F-9, Harbor-UCLA Medical Center, Torrance, California 90509

ABSTRACT Several mathematical formulas are presented for estimating regional average circumferential stress and shear stress in a thick-wall, noncircular cylinder with a plane of symmetry. The formulas require images of exterior and interior chamber silhouettes plus surface pressures. The formulas are primarily intended for application to the left ventricle in the short axis plane near the base (where the meridional radius of curvature is normally much larger than the circumferential radius of curvature) and to blood vessels. The formulas predict stresses in a variety of chambers to within 3% of finite element values determined from a large-scale structural analysis computer program called ANSYS.

INTRODUCTION

Based on our knowledge of structures in general, we know that stress varies with position depending on regional geometry, loading, and material properties. When data are available on these quantities, reliable predictions of stress can be obtained albeit with complex software and powerful mainframe computers. However, data on regional geometry, loading, and material properties for the left ventricle are only partially available.

Experimentally, it has been found that estimates of wall stress correlate with important physiologic events in the heart, such as left ventricular ischemia and left ventricular hypertrophy in a wide range of normal and pathologic states. Thus, improved methods of estimating left ventricular wall stress would have important physiologic and clinical implications. With the rapid technical advances in image acquisition and processing in recent years (Robb, 1985), it has become possible to obtain high-resolution data on regional geometry with relatively little risk to the patient. Short axis images are particularly important in the study of left ventricular function for two reasons. First, they are usually of better quality, so that endocardial and epicardial definition are more accurate and reproducible. Second, the distribution of all the major coronary arteries can be visualized in a single short axis image so that the effects of regional ischemia can be readily ascertained. Although not routine, simultaneous measurements of cavity pressure (i.e., loading) are also technically feasible. The biggest source of uncertainty is in the area of regional material properties.

Address for Correspondence R. F. Janz Advanced Technology, Inc. 222 N. Sepulveda Blvd. Suite 1310 El Segundo, CA 90245.

Extensive measurements of one-dimensional material properties have been made with passive and active animal papillary muscles. However, severe technical problems have limited multidimensional research, although significant progress has been made in the acquisition of two-dimensional data for passive dog myocardium (Demer and Yin, 1983; Yin et al., 1986).

Attempts to reconstruct the required three-dimensional properties from one-dimensional papillary muscle data and measurements of fiber orientation in animal hearts generally assume the fiber direction is a principal direction (implying shear stresses in a coordinate system aligned with the fiber direction are equal to zero) and stresses transverse to the fiber direction are equal to the local hydrostatic pressure (e.g., Tozeren, 1983). While these two assumptions seem plausible, recent measurements of regional strain indicate that at least the first one may not be strictly valid (Waldman, et al. 1985). In any case, the applicability of this approach for the purpose of determining regional stress seems remote at the present time in that it will take a large number of parameters to define the three-dimensional behavior of a material as complex as the myocardium which exhibits both passive and active, directionally dependent properties that degrade regionally with disease.

The lack of data on three-dimensional myocardial material properties plus considerations of computational economy and insight provided by closed-form mathematical formulas have promoted the wide spread use of various versions of LaPlace's law for predicting stress (Mirsky, 1979; Huisman et al., 1980; Yin, 1981). This law takes advantage of the fact that stresses in statically determinate structures such as thin-wall spheres, cylinders, and ellipsoids are characterized completely by conditions of equilibrium (i.e., force balances).

Although the left ventricle does not fall within this category of structures these methods have been used for estimating global average stress, or average stress at the base of the ventricle in clinical studies since they do not require knowledge of the myocardial material properties (e.g., Mirsky et al., 1983; DePace et al., 1983; St. John Sutton et al., 1984; Zile et al., 1984; Douglas and Reichek, 1986).

The methodology suggested by LaPlace's law was recently extended to include the estimation of average circumferential and meridional stress at arbitrary locations in a thick-wall solid with circular cross section in the short axis plane (Janz, 1982). One of the first applications for this new formulation involved an analysis of relaxation in patients with coronary artery disease (Pouleur et al., 1984). However, in spite of the enhanced flexibility of this formulation relative to previous models, it too was limited by the unrealistic assumptions of circular symmetry and negligible shear stress.

In this paper we address the absence of circular symmetry and the presence of shear stress in the left ventricle. Surprisingly enough, the results have a simple geometric interpretation in spite of the rigorous treatment. Of particular significance is the introduction of a new geometric parameter that replaces radius of curvature in the membrane theory of cylindrical shells. At the same time, we point out that the results represent only another step in the application of the Laplace methodology. They should not be used indiscriminately at arbitrary locations in the ventricular wall.

METHODS

Two equations for circumferential stress (σ_ψ), shear stress ($\tau_{R\psi}$), and stress normal (σ_R) to the inner surface of a hollow, thick-wall cylinder with noncircular cross section are derived in Appendix A by equating opposing forces on an infinitesimal volume element. Since we neglect inertia, we are assuming that static equilibrium is achieved at each instant in time. Although these two equations are inadequate to specify the positional dependence of all three-stresses, we show by elementary mathematical methods in Appendix B that they are adequate to specify the positional dependence of σ_ψ and $\tau_{R\psi}$ averaged across the wall of the cylinder. We also provide a simple geometric interpretation of our results in Appendix B. For the convenience of the reader, we summarize all assumptions pertaining to our results in Table 1.

Unfortunately, the present lack of reliable experimental techniques for measuring regional stresses in the left ventricle precludes direct validation of our results. However, we have attempted to demonstrate the plausibility of our findings by comparisons with other independent theoretical results.

We have surveyed the literature and except for the circular cylinder there appear to be no other relevant analytical results which are available to serve as bench marks. (For the circular cylinder $L = R$ and $dL/d\psi = dR/d\psi = 0$ in Eqs. B13 and B14 in Appendix B. We therefore obtain the correct result for this limiting case.) Consequently, we have created a series of three test cases of increasing complexity for which it is possible to obtain numerical results using the finite element method

TABLE 1 Summary of assumptions in theoretical models

Assumption	Analytical formulas	Finite element cases
Neglect inertia	Yes	Yes
Zero stresses in axial direction	Yes	Yes
Plane of symmetry	Yes	Yes
Uniform wall thickness	Yes	1, 2
Uniform surface pressures	Yes	Yes
Isotropic	*	Yes
Passive	*	Yes
Nearly incompressible	*	Yes
Homogeneous	*	Yes

*Not relevant.

(Heethaar et al., 1976; Janz and Waldron, 1978; McPherson et al., 1987). For this purpose we chose to use a computer program called ANSYS developed by Swanson Analysis Systems, Inc. (Houston, PA), and the CYBER 170/760 computer. Since the finite element method requires a specification of material properties, for simplicity we chose a linear, homogeneous, isotropic material for the test cases with a ratio of cavity pressure to Young's modulus which assured small strains and displacements. All cases were based on ANSYS element number 42 (two-dimensional isoparametric solid element).

We checked the adequacy of our finite element meshes by computing stresses in a thick-wall, hollow circular cylinder. Agreement to within 1% of the Lame' solution was considered adequate.

For the purposes of comparing the finite element results with Eqs. B13 and B14, we also wrote a small computer program for the IBM Personal Computer which determines average stresses predicted by these equations from the regional wall geometry of the finite element models and their surface pressures, transforms the finite element stresses element-by-element from the ANSYS Cartesian (x-y) coordinate system to the $R - \psi$ coordinate system introduced in Appendix A, and averages the transformed stresses across the wall at selected positions.

RESULTS

The main results of this study consist of formulas for estimating regional average circumferential stress ($\bar{\sigma}_\psi(\psi)$) and shear stress ($\bar{\tau}_{R\psi}(\psi)$) in a thick-wall, noncircular cylinder with a plane of symmetry. They are derived in the appendixes and presented in their most general form by Eqs. B9–B12. These formulas involve two classes of parameters: (1) pressures (internal and external to the chamber cavity), and (2) chamber dimensions (refer to Figs. B2 and B3). The latter quantities may be estimated from a short axis image of the chamber.

We evaluated these formulas theoretically by comparing stresses predicted by the formulas with corresponding stresses obtained from three finite element models of noncircular cylinders of increasingly complex shape ranging from an elliptical cylinder of uniform wall thickness to a cylinder of nonuniform wall thickness whose shape is based on a short axis echocardiographic image of the dog left ventricle obtained near the base. In each of the three

finite element models, the outer surface pressure (P_o) was set equal to zero.

The first of the finite element models is the elliptical cylinder of uniform wall thickness shown in Fig. 1. Average circumferential stresses at three positions were determined from the finite elements highlighted in this figure. (Since the formulas determine average stress along a perpendicular to the interior wall of the chamber, the highlighted elements correspond to those that intersect this perpendicular at the indicated angle, ψ. In some instances, the intersection involves two adjacent elements in a given concentric layer of elements. When this occurs, stresses in the adjacent elements are also included in the average finite element stress calculation.) They were compared with stresses predicted by Eq. B27. As indicated in Table 2, the stresses at all three positions agreed to within 1%.

The second finite element model is the more complex cylinder of uniform wall thickness shown in Fig. 2. Average circumferential stresses at five positions were determined from the highlighted finite elements. They were compared with stresses predicted by Eq. B25 (identical results would have been obtained if we had used Eqs. B21 or B23) with $\bar{\sigma}_\psi(0)$ and $\bar{\sigma}_\psi(\pi)$ determined from Eqs. B17 and B18 and y_o and y_π determined from Eqs. B19 and B20. As indicated in Table 2, the maximum difference in stresses for the five positions was 2% at positon 3.

The third finite element model is the cylinder of nonuniform wall thickness shown in Fig. 3. Average circumferential stresses at five positions were determined from the highlighted finite elements. They were compared with stresses predicted by the following formulas. For positions 1 and 2, Eq. B21 was used with $\bar{\sigma}_\psi(0)$ determined from Eq. B17, y_o and y_π determined from Eqs.

TABLE 2 Comparison of regional average circumferential stresses predicted by mathematical formulas and ANSYS finite element computer program

	$\bar{\sigma}_\psi(\psi)/\Delta P^*$	
	Mathematical (equation)	ANSYS
Elliptical cylinder (Fig. 1)		
Position 1 ($\psi = 0°$)	2.00 (B27)	2.00
Position 2 ($\psi = 67.8°$)	1.21 (B27)	1.20
Position 3 ($\psi = 90°$)	1.00 (B27)	1.00
Less symmetrical cylinder/uniform wall thickness (Fig. 2)		
Position 1 ($\psi = 0°$)	1.47 (B25)	1.46
Position 2 ($\psi = 52.7°$)	1.11 (B25)	1.11
Position 3 ($\psi = 91.2°$)	1.27 (B25)	1.30
Position 4 ($\psi = 137.6°$)	1.30 (B25)	1.28
Position 5 ($\psi = 180°$)	1.20 (B25)	1.20
Less symmetrical cylinder/nonuniform wall thickness (Fig. 3)		
Position 1 ($\psi = 0°$)	1.42 (B21)	1.39
Position 2 ($\psi = 52.7°$)	1.07 (B21)	1.07
Position 3 ($\psi = 95.8°$)	1.55 (B23)	1.50
Position 4 ($\psi = 142.6°$)	1.95 (B23)	1.92
Position 5 ($\psi = 180°$)	2.24 (B23)	2.27

*Since the outer surface pressure (P_o) was set equal to zero, transmural pressure (ΔP) is equal to the inner surface pressure.

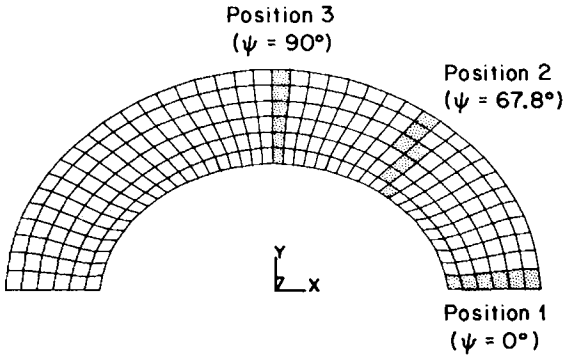

FIGURE 1 Finite element model for an elliptical cylinder. The angle denoted ψ is the angle between the x-axis and a perpendicular to the interior wall of the chamber. Average circumferential stresses determined from the highlighted finite elements were compared with average stresses predicted by one of the formulas presented in this article at the three values of ψ indicated in the figure.

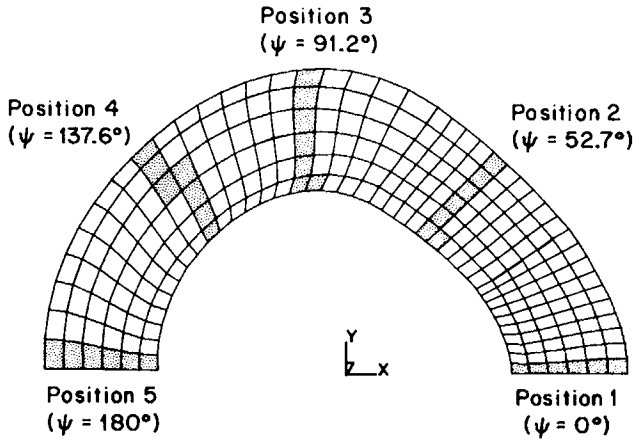

FIGURE 2 Finite element model for a cylinder of uniform wall thickness with one plane of symmetry ($\psi = 0$). Average circumferential stresses determined from the highlighted finite elements were compared with average stresses predicted by the formulas presented in this article at the five values of ψ indicated in the figure.

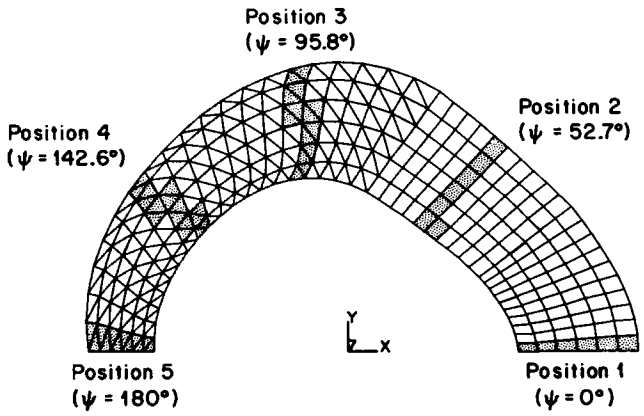

FIGURE 3 Finite element model for a cylinder of nonuniform wall thickness with one plane of symmetry ($\psi = 0$) based on a short axis echocardiographic image of the dog left ventricle obtained near the base. Average circumferential stresses determined from the highlighted finite elements were compared with average stresses predicted by the formulas presented in this article at the five values of ψ indicated in the figure.

B19 and B20, and wall thickness (T) in the denominator of the third term in the coefficient of cos ψ set equal to its value at position 1. For positions 3, 4, and 5, Eq. B23 was used with $\bar{\sigma}_\psi(\pi)$ determined from Eq. B18, and the corresponding value of wall thickness (T) set equal to its value at position 5. As indicated in Table 2, the maximum difference in stresses for the five positions was 3% at position 3.

As indicated in Appendix B, for cylinders with uniform wall thickness and one plane of symmetry (Fig. 2) Eqs. B21, B23, and B25 all give equivalent results. For cylinders with nonuniform wall thickness and one plane of symmetry (Fig. 3), it is recommended that either Eq. B21 or B23 be used depending on whether the position (ψ) of interest is closer to $\psi = 0$ or $\psi = \pi$. In either case, two different wall thicknesses are used in the equations. The coefficient of cos ψ requires the wall thickness at $\psi = 0$ (Eq. B21) or $\psi = \pi$ (Eq. B23). The remaining wall thickness appearing in the term $\Delta PL/T$ in either of these two equations should be interpreted as wall thickness at the position (ψ) of interest. For cylinders with two planes of symmetry (Fig. 1) Eqs. B21, B23, B25, and B27 all give equivalent results since the coefficients of cos ψ in Eqs. B21, B23, and B25 are all equal to zero.

DISCUSSION

In a previous study (Janz, 1982) two formulas were presented for estimating regional average circumferential stress in an axisymmetric model of the left ventricular chamber. This was an initial attempt to extend the LaPlace methodology to a more realistic representation of ventricular geometry in the long axis plane than previously reported. This extension, however, was limited by the assumptions of circular symmetry in the short axis plane and negligible shear stress.

In the present study we focus on a more realistic representation of ventricular geometry in the short axis plane than previously reported and account for the presence of shear stress. The formulas presented in this paper are therefore intended to compliment rather than replace those of the previous study. Unfortunately, the new formulas also have their limitations. The most restrictive of these is their applicability only to regions where the meridional radius of curvature in the long axis plane is very large compared with short axis cavity dimensions and wall thickness. This restriction generally limits their application to regions near the base of the ventricle.

In addition to their surprising simplicity, the most significant theoretical aspect of the new formulas is their dependence on the geometric parameter, L, illustrated in Fig. B2. This parameter replaces circumferential radius of curvature which appears in formulas based on the membrane theory of noncircular cylinders. This difference in the dependence of stress on shape is significant for two reasons. First, and most importantly, in cylinders such as the one shown in Fig. 1 membrane theory would predict a higher value for average circumferential stress at position 3 rather than position 1 because of the relative magnitudes of the radii of curvature at these two locations. However, the thick-wall theory presented in this study predicts an average circumferential stress at position 3 which is a factor of 2 lower than the value at position 1 owing to the relative magnitude of L. Second, the parameter L can be determined numerically in a relatively simple manner from its definition in Eq. B29. Radii of curvature are more difficult to determine with acceptable accuracy from digitized contours.

The remarkable agreement in stresses predicted by the simple formulas presented in this study and those predicted by an industry standard finite element computer program provides evidence of their theoretical validity. The favorable agreement in the third test case (Fig. 3) indicates that the formulas may also be applied beyond their theoretical range of applicability which includes a restriction to cylinders with uniform wall thickness (refer to Table 1). To what extent the conditions associated with a plane of symmetry and large meridional radius of curvature relative to short axis dimensions can also be relaxed remains to be determined. Further comparisons with other finite element results are required to more fully establish the limitations of the formulas.

Several additional observations need to be made relative to the application of the formulas presented in this study to the left ventricle. (1) It would be desirable to

have a condition that provides a quantitative estimate of how large the meridional radius of curvature in the long axis plane needs to be before meaningful estimates of regional stress can be obtained with these formulas. An exact determination of this condition would require a three-dimentional analysis. However, an indication of the nature of this condition can be obtained from our previous axisymmetric analysis (Janz, 1982). The formula we presented in that study for average circumferential stress may be written in the following way (modified slightly to account for transmural pressure):

$$\bar{\sigma}_\psi + P_o = \frac{\Delta P r}{T}\left\{\frac{1 - r/(2R_\phi \sin\phi)}{\sin\phi[1 + T/(2R_\phi)]}\right\},$$

where P_o = outer surface pressure, ΔP= transmural pressure, r = circumferential radius of curvature, T = wall thickness, ϕ = angle between long axis and perpendicular to inner wall in long axis plane, and R_ϕ = meridional radius of curvature. From this equation we can determine how large R_ϕ has to be relative to r and T for average circumferential stress in a circular cylinder ($\Delta Pr/T$) to be a good approximation to average circumferential stress in an axisymmetric solid at a given location, ϕ. For example, for $r/R_\phi = T/R_\phi = 0.05$, $\Delta Pr/T$ would overestimate $\bar{\sigma}_\psi + P_o$ at $\phi = 85°$ by 5%.

(2) Stresses in the heart wall will, in general, include elastic, viscous, contractile, and hydrostatic components. However, the regional stresses predicted by our formulas (as well as the global stresses predicted by Laplace's law) represent the net combination of all of these component stresses. Currently we have no way of determining, for example, what fraction of the stress predicted by our formulas is due to active contraction or passive extension of elastic elements (except for a qualitative determination based on the phase of the cardiac cycle). We do know, however, that all of these stress components relate directly to the muscle fiber except for the hydrostatic component which arises from the incompressibility of the myocardium. Consequently, if the stresses predicted by our formulas are to be interpreted as fiber stresses, the formulas need to be corrected for the hydrostatic component.

Several investigators have evaluated the assumption that stress in a direction perpendicular to the interior surface is purely hydrostatic (Streeter et al., 1970; Janz and Waldron, 1976; Arts et al., 1979; Tozeren, 1983). We also know that this stress is compressive (negative) and varies continuously in absolute value between the two surface pressures. If this variation is linear and normal stress is indeed purely hydrostatic, average normal stress will be equal to the negative of the average of the two surface pressures.

In Appendix C we attempt to eliminate the hydrostatic component from our formulas by subtracting an expression for normal stress (based on the assumptions that this stress is purely hydrostatic and varies linearly with distance through the wall) from total circumferential stress. Although the resulting formulas (C3–C6) represent an attempt to relate total stress more closely to fiber stress, the expression for normal stress is not based on the same theoretical foundation as the formulas for total stress (B21–B28), which are the main results of this study.

(3) If average circumferential stress (properly adjusted for the hydrostatic component) is actually attained near midwall, it may be interpreted as fiber stress since the dominant fiber direction at midwall is circumferential (Streeter et al., 1969). Whether or not average stress is a good estimate of midwall stress depends on the (unknown) stress distribution across the wall. We conducted a review of theoretical circumferential stress distributions ranging from those which are monotonic as in the Lamé cylinder, to those which are not as in some of the more recent "fiber" models (e.g., Tozeren, 1983; Jan, 1985) and found that regardless of the model, average circumferential stresses consistently occurred very near the midwall. We therefore interpret stresses predicted by Eqs. B21–B28 as total stress in the fiber direction at midwall, and stresses predicted by Eqs. C3–C6 as approximations for midwall fiber stress.

(4) It is not recommended that either of the above sets of formulas be applied in their current form across the junctions between the two ventricles because of the discontinuity in exterior pressure on the free wall relative to the septum. As indicated in Table 1 the theoretical development presented in this study is based on the assumption of uniform internal and external surface pressure.

SUMMARY

In spite of the limitations discussed above relative to the quantitative application of the newly derived formulas for stress to the left ventricle, these formulas are capable of predicting stresses in noncircular cylinders of nonuniform wall thickness with remarkable accuracy. In addition, the emergence of another geometric parameter as a replacement for radius of curvature may provide new qualitative insight into the significance of both chronic and acute geometric changes as possible mechanisms for ventricular compensation.

APPENDIX A

Derivation of equilibrium equations

Neglecting inertia, the forces acting on an infinitesimal volume element of an asymmetrical cylindrical chamber of unit height are shown in Fig. A1. Equating opposing forces in the circumferential direction we obtain, after some manipulation, the following equation relating circumferen-

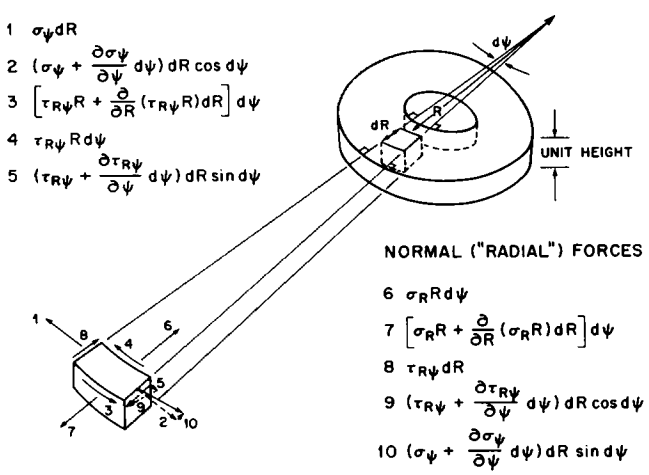

FIGURE A1 Forces acting on an infinitesimal volume element in a cylinder of arbitrary cross section and unit height. R denotes radius of curvature and ψ denotes the angle between an arbitrary reference perpendicular at the interior wall and the perpendicular at a position of interest.

tial stress (σ_ψ) to shear stress ($\tau_{R\psi}$):

$$\frac{\partial \sigma_\psi}{\partial \psi} + \frac{\partial}{\partial R}(R\tau_{R\psi}) + \tau_{R\psi} = 0. \tag{A1}$$

Equating opposing forces in a direction normal to the interior surface, we obtain an equation relating circumferential stress and shear stress to the normal stress (σ_R):

$$\frac{\partial (R\sigma_R)}{\partial R} + \frac{\partial (\tau_{R\psi})}{\partial \psi} - \sigma_\psi = 0. \tag{A2}$$

With hydrostatic pressure acting on the inner and outer surfaces of the cylinder, we also need to impose four other mathematical conditions.

$$\left.\begin{aligned} \sigma_R &= -P_i \\ \tau_{R\psi} &= 0 \end{aligned}\right\} \text{on the inner surface}$$

$$\left.\begin{aligned} \sigma_R &= -P_o \\ \tau_{R\psi} &= 0 \end{aligned}\right\} \text{on the outer surface,} \tag{A3}$$

where P_i and P_o denote inner and outer surface pressures, respectively.

Although the above two equations and four conditions do not uniquely characterize the positional dependence of all three stresses, as shown in Appendix B they are adequate to uniquely define the circumferential stress and shear stress averaged across the wall of the cylinder.

APPENDIX B

Derivation of formulas for regional average stresses

We begin with the following definitions:

Wall thickness (T)

$$T = \int_{R_i}^{R_o} dR = R_0 - R_i,$$

where R_o and R_i denote the outer and inner radii of curvature for a given value of ψ.

Average circumferential stress ($\bar{\sigma}_\psi$)

$$\bar{\sigma}_\psi = \frac{1}{T}\int_{R_i}^{R_o} \sigma_\psi dR$$

Average shear stress ($\bar{\tau}_{R\psi}$)

$$\bar{\tau}_{R\psi} = \frac{1}{T}\int_{R_i}^{R_o} \tau_{R\psi} dR$$

Transmural pressure (ΔP)

$$\Delta P = P_i - P_o$$

Integrating Eq. A1 with respect to R between R_i and R_o, we obtain the following result for a cylinder with uniform wall thickness:

$$\frac{d\bar{\sigma}_\psi}{d\psi} + \bar{\tau}_{r\psi} = 0. \tag{B1}$$

Integrating Eq. A2 with respect to R between R_i and R_o we obtain the following result by using the relationship $R_o = R_i + T$ and dropping the subscript, i, on the inner radius of curvature:

$$\frac{d\bar{\tau}_{R\psi}}{d\psi} - \bar{\sigma}_\psi = -\frac{\Delta PR}{T} + P_o. \tag{B2}$$

Eqs. B1 and B2 can be uncoupled by differentiating with respect to ψ and combining results. At this point we also make the additional assumption that the surface pressures are uniform.

$$\frac{d^2\bar{\sigma}_\psi}{d\psi^2} + \bar{\sigma}_\psi = \frac{\Delta PR}{T} - P_o \tag{B3}$$

$$\frac{d^2\bar{\tau}_{R\psi}}{d\psi^2} + \bar{\tau}_{R\psi} = -\frac{\Delta P}{T}\frac{dR}{d\psi}. \tag{B4}$$

Eqs. B3 and B4 can be solved by standard methods for ordinary differential equations. The results are as follows:

$$\bar{\sigma}_\psi(\psi) + P_o = [\bar{\sigma}_\psi(0) + P_o]\cos\psi - \bar{\tau}_{R\psi}(0)\sin\psi + \frac{\Delta P}{T}\left(\sin\psi\int_0^\psi R\cos\xi d\xi - \cos\psi\int_0^\psi R\sin\xi d\xi\right) \tag{B5}$$

$$\bar{\tau}_{R\psi}(\psi) = [\bar{\sigma}_\psi(0) + P_o]\sin\psi + \bar{\tau}_{R\psi}(0)\cos\psi - \frac{\Delta P}{T}\left(\sin\psi\int_0^\psi R\sin\xi d\xi + \cos\psi\int_0^\psi R\cos\xi d\xi\right). \tag{B6}$$

At this point in the discussion, $\psi = 0$ corresponds to an arbitrary reference position, and Eqs. B5 and B6 completely define the average circumferential and shear stresses ($\bar{\sigma}_\psi(\psi)$ and $\bar{\tau}_{R\psi}(\psi)$) relative to their values at this position ($\sigma_\psi(0)$ and $\bar{\tau}_{R\psi}(0)$). In this form, however, the results are too complex for routine implementation, and they offer little insight into the nature of the primary determinants of wall stress. To further simplify these results we use the two elementary relations from differential geometry shown in Fig. B1. In this figure we have superimposed a Cartesian coordinate system aligned with the reference position ($\psi = 0$) on a short axis view of a portion of the inner surface of the cylinder. Substituting $dx/d\xi$ for $R\cos\xi$ and $-dy/d\xi$ for $R\sin\xi$ in Eqs.

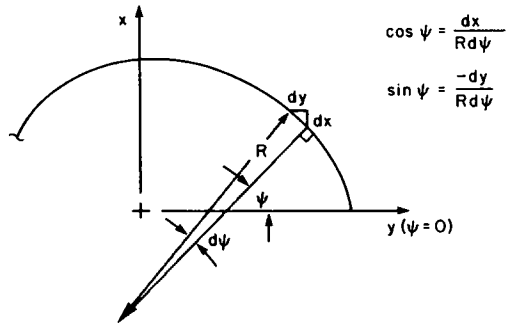

FIGURE B1 Portion of the inner surface of a noncircular cylinder. Two differential equations for the cartesian coordinates x and y in terms of R and ψ are readily derived from this figure.

B5 and B6 and performing all integrations we obtain the following results:

$$\bar{\sigma}_\psi(\psi) + P_o = \left[\bar{\sigma}_\psi(0) + P_o - \frac{\Delta P y(0)}{T}\right]\cos\psi - \bar{\tau}_{R\psi}(0)\sin\psi + \frac{\Delta P}{T}[x(\psi)\sin\psi + y(\psi)\cos\psi] \quad \text{(B7)}$$

$$\bar{\tau}_{R\psi}(\psi) = \left[\sigma_\psi(0) + P_o - \frac{\Delta P y(0)}{T}\right]\sin\psi + \bar{\tau}_{R\psi}(0)\cos\psi - \frac{\Delta P}{T}[x(\psi)\cos\psi - y(\psi)\sin\psi]. \quad \text{(B8)}$$

From a computational point of view, these two equations are much simpler than Eqs. B5 and B6. Part of this simplification is due to the absence of radius of curvature in both equations. In fact, radius of curvature has been replaced by the quantity $[x(\psi)\sin\psi + y(\psi)\cos\psi]$ as the second (next to wall thickness) primary geometric determinant of wall stress. Referring to Fig. B2 we see that this quantity has a simple geometric interpretation.

Since $x = \xi\sin\psi$ and $y = \Delta + \xi\cos\psi$, $x\sin\psi + y\cos\psi = \xi + \Delta\cos\psi = L$. The quantity, L, as defined in this figure should be used in place of radius of curvature for determining stress in noncircular cylinders.

Substituting back into Eqs. B7 and B8 we get the following results:

$$\bar{\sigma}_\psi(\psi) + P_o = \left[\bar{\sigma}_\psi(0) + P_o - \frac{\Delta P y(0)}{T}\right]\cos\psi - \bar{\tau}_{R\psi}(0)\sin\psi + \frac{\Delta P L}{T} \quad \text{(B9)}$$

$$\bar{\tau}_{R\psi}(\psi) = \left[\bar{\sigma}_\psi(0) + P_o - \frac{\Delta P y(0)}{T}\right]\sin\psi + \bar{\tau}_{R\psi}(0)\cos\psi - \frac{\Delta P}{T}\frac{dL}{d\psi}. \quad \text{(B10)}$$

If we had chosen $\psi = \pi$ as our reference position we would have obtained the following equivalent forms of Eqs. B9 and B10 by a completely analogous procedure:

$$\bar{\sigma}_\psi(\psi) + P_o = -\left[\bar{\sigma}_\psi(\pi) + P_o - \frac{\Delta P|y(\pi)|}{T}\right]\cos\psi + \bar{\tau}_{R\psi}(\pi)\sin\psi + \frac{\Delta P L}{T} \quad \text{(B11)}$$

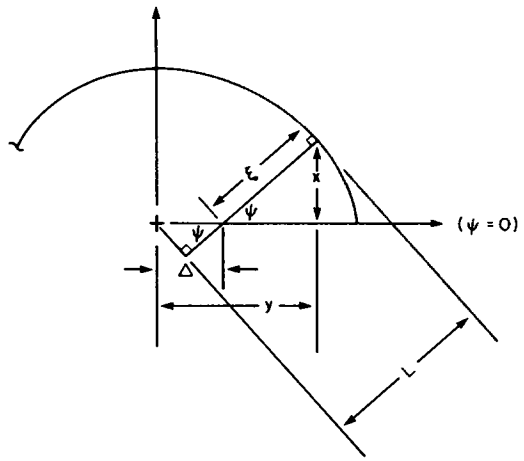

FIGURE B2 Portion of the inner surface of a noncircular cylinder illustrating the geometric quantity, L, a major determinant of stress.

$$\bar{\tau}_{R\psi}(\psi) = -\left[\bar{\sigma}_\psi(\pi) + P_o - \frac{\Delta P|y(\pi)|}{T}\right]\sin\psi - \bar{\tau}_{R\psi}(\pi)\cos\psi - \frac{\Delta P}{T}\frac{dL}{d\psi}. \quad \text{(B12)}$$

We consider Eqs. B9–B12 to be our primary theoretical result. However, we are still unable to apply them until we use some other conditions which will allow us to specify the stresses at our reference positions (i.e., either $\bar{\sigma}_\psi(0)$ and $\bar{\tau}_{R\psi}(0)$ or $\bar{\sigma}_\psi(\pi)$ and $\bar{\tau}_{R\psi}(\pi)$). We choose to assume that our noncircular cylinder has a plane of symmetry. The manner in which this assumption allows us to determine $\bar{\sigma}_\psi(0)$, $\bar{\tau}_{R\psi}(0)$, $\bar{\sigma}_\psi(\pi)$, and $\bar{\tau}_{R\psi}(\pi)$ is discussed below.

As indicated in Fig. B3*a*, we take the reference position ($\psi = 0$) along the plane of symmetry. For the sake of generality we will develop the needed conditions for a noncircular cylinder with a nonuniform wall thickness. We first observe that because of symmetry $d\bar{\sigma}_\psi/d\psi$ and $\bar{\tau}_{R\psi}$ are both equal to zero at $\psi = 0$ and $\psi = \pi$. We show the remaining forces (and two new dimensions defined later) acting on a free-body diagram of the upper half of the cylinder in Fig. B3*b*. (Recall that we take the cylinder to be of unit height.) One condition is immediately apparent from the free-body diagram. Equating forces in the vertical (i.e., $\psi = \pi/2$) direction we obtain:

$$T_o\bar{\sigma}_\psi(0) + T_\pi\bar{\sigma}_\psi(\pi) = \Delta P[y(0) + |y(\pi)|] - P_o(T_o + T_\pi). \quad \text{(B13)}$$

We obtain a second condition by equating moments about the origin to zero. However, before doing this, we first define the two dimensions, y_o and y_π shown in Fig. B3*b*, as follows:

$$y_o = \frac{\int_{y(0)}^{y(0)+T_o}\sigma_\psi(y)|_{\psi=0}\,y\,dy}{\int_{y(0)}^{y(0)+T_o}\sigma_\psi(y)|_{\psi=0}\,dy} \quad \text{(B14)}$$

$$y_\pi = \frac{\int_{|y(\pi)|}^{|y(\pi)|+T_\pi}\sigma_\psi(y)|_{\psi=\pi}\,y\,dy}{\int_{|y(\pi)|}^{|y(\pi)|+T_\pi}\sigma_\psi(y)|_{\psi=\pi}\,dy} \quad \text{(B15)}$$

That is, they are defined in such a way that the quantities $y_oT_o\bar{\sigma}_\psi(0)$ and $y_\pi T_\pi\bar{\sigma}_\psi(\pi)$ are the clockwise and counterclockwise moments, respectively, about the origin of the upper half of the cylinder shown in Fig.

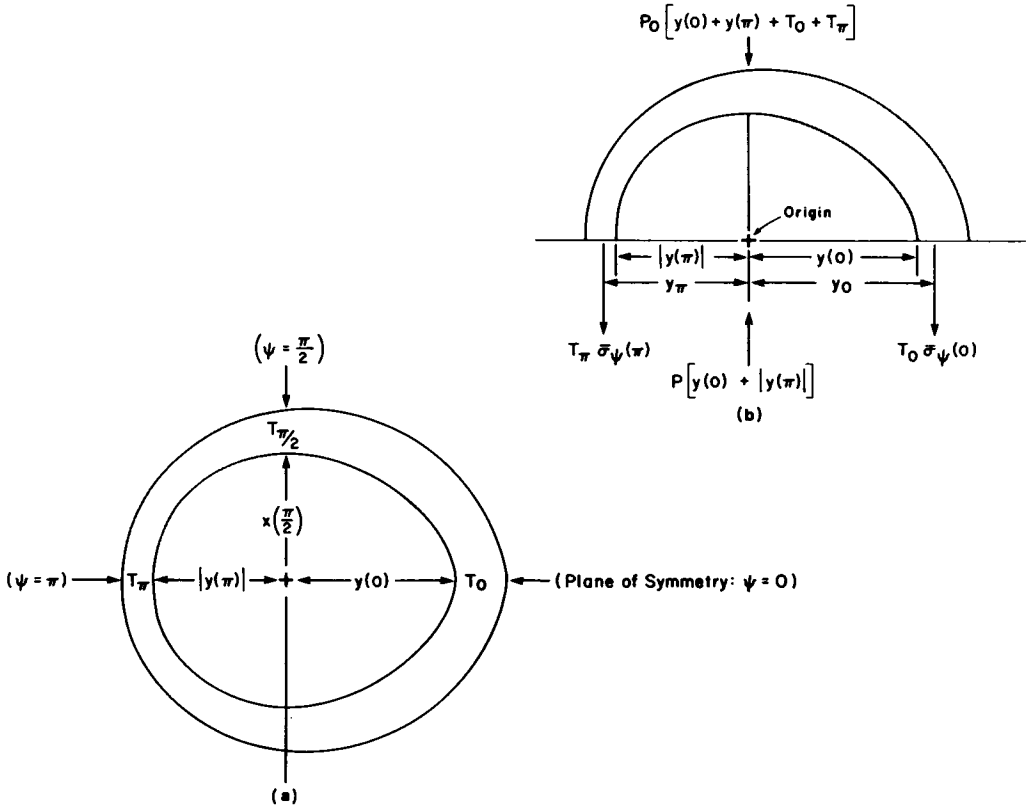

FIGURE B3 (*a*) Geometric parameters in mathematical conditions required for a unique determination of stress. (*b*) Free-body diagram illustrating the forces acting on a noncircular cylinder with nonuniform wall thickness and a single plane of symmetry ($\psi = 0$).

B3*b* owing to circumferential stresses acting at $\psi = 0$ and $\psi = \pi$. The second condition may therefore be stated as follows:

$$y_o T_o \bar{\sigma}_\psi(0) - y_\pi T_\pi \bar{\sigma}_\psi(\pi) = \frac{P}{2}[y^2(0) - y^2(\pi)] - \frac{P_o}{2}\{[y(0) + T_o]^2 - [y(\pi) + T_\pi]^2\}. \quad \text{(B16)}$$

We can obtain $\bar{\sigma}_\psi(0)$ and $\bar{\sigma}_\psi(\pi)$ by solving Eqs. B13 and B16. The results are as follows:

$$\bar{\sigma}_\psi(0) = \frac{P[y(0) + |y(\pi)|]}{T_o(y_o + y_\pi)}\left[y_\pi + \frac{y(0) - |y(\pi)|}{2}\right] - \frac{P_o[y(0) + T_o + |y(\pi)| + T_\pi]}{T_o(y_o + y_\pi)} \cdot \left\{y_\pi + \frac{y(0) + T_o - [|y(\pi)| + T_\pi]}{2}\right\} \quad \text{(B17)}$$

$$\bar{\sigma}_\psi(\pi) = \frac{P[y(0) + |y(\pi)|]}{T_\pi(y_o + y_\pi)}\left\{y_o - \frac{[y(0) - |y(\pi)|]}{2}\right\} - \frac{P_o[y(0) + T_o + |y(\pi)| + T_\pi]}{T_\pi(y_o + y_\pi)} \cdot \left[y_o - \left\{\frac{y(0) + T_o - [|y(\pi)| + T_\pi]}{2}\right\}\right]. \quad \text{(B18)}$$

While these expressions for $\bar{\sigma}_\psi(0)$ and $\bar{\sigma}_\psi(\pi)$ may seem complex, they are simple to evaluate, numerically, provided we have all the required parameters. We assume that the pressures (P and P_o), thicknesses (T_o and T_π) and the dimension $y(0) + |y(\pi)|$ can be measured. We choose the origin to correspond to the point where $\psi = \pi/2$ as shown in Fig. B3. Once the origin has been selected, individual values for $y(0)$ and $|y(\pi)|$ are determined. The remaining parameters required are y_o and y_π. They cannot be evaluated from their definitions (Eqs. B14 and B15) because the variation in σ_ψ across the wall cannot be determined from conditions of equilibrium alone. This variation will depend on the properties of the material in the wall of the cylinder. We resort to the following empirical formulas for y_o and y_π:

$$y_o = (1 - \alpha)y(0) + \alpha|y(\pi)| + \beta T_o \quad \text{(B19)}$$

$$y_\pi = \alpha y(0) + (1 - \alpha)|y(\pi)| + \beta T_\pi, \quad \text{(B20)}$$

where, α and β are constants. For the cylinders considered in this article, we have found that $\alpha = 1/4$ and $\beta = 1/3$ work well.

At this point we would like to make several observations regarding the above results.

First of all, as noted earlier, with a plane of symmetry at $\psi = 0$ (or π), the shear stresses along this plane are equal to zero. Therefore Eqs. B9–B12 may be simplified as follows:

$$\bar{\sigma}_\psi(\psi) + P_o = \left[\bar{\sigma}_\psi(0) + P_o - \frac{\Delta P y(0)}{T}\right]\cos\psi + \frac{\Delta P L}{T} \quad \text{(B21)}$$

$$\bar{\tau}_{R\psi}(\psi) = \left[\bar{\sigma}_\psi(0) + P_o - \frac{\Delta P y(0)}{T}\right]\sin\psi - \frac{\Delta P}{T}\frac{dL}{d\psi} \quad \text{(B22)}$$

$$\bar{\sigma}_\psi(\psi) + P_o = -\left[\bar{\sigma}_\psi(\pi) + P_o - \frac{\Delta P|y(\pi)|}{T}\right]\cos\psi + \frac{\Delta PL}{T} \quad \text{(B23)}$$

$$\bar{\tau}_{R\psi}(\psi) = -\left[\bar{\sigma}_\psi(\pi) + P_o - \frac{\Delta P|y(\pi)|}{T}\right]\sin\psi - \frac{\Delta P}{T}\frac{dL}{d\psi}. \quad \text{(B24)}$$

An alternate form for these formulas which suggests a further simplification may be obtained by adding corresponding formulas and dividing by two. Proceeding along these lines we obtain:

$$\bar{\sigma}_\psi(\psi) + P_o = \left\{\frac{\bar{\sigma}_\psi(0) - \bar{\sigma}_\psi(\pi)}{2} - \frac{\Delta P}{T}\frac{[y(0) - |y(\pi)|]}{2}\right\} \cdot \cos\psi + \frac{\Delta PL}{T} \quad \text{(B25)}$$

$$\bar{\tau}_{R\psi}(\psi) = \left\{\frac{\bar{\sigma}_\psi(0) - \bar{\sigma}_\psi(\pi)}{2} - \frac{\Delta P}{T}\frac{[y(0) - |y(\pi)|]}{2}\right\} \cdot \sin\psi - \frac{\Delta P}{T}\frac{dL}{d\psi}. \quad \text{(B26)}$$

Therefore, if in addition to a plane of symmetry at $\psi = 0$ (or π), we also have a plane of symmetry at $\psi = \pi/2$ such as for an elliptical cylinder for which $\bar{\sigma}_\psi(0) = \bar{\sigma}_\psi(\pi)$ and $y(0) = |y(\pi)|$, we obtain a surprisingly compact set of formulas (note the similarity between Eq. B27 and LaPlace's law for a thick-wall circular cylinder or a noncircular cylindrical membrane):

$$\bar{\sigma}_\psi(\psi) + P_o = \frac{\Delta PL}{T} \quad \text{(B27)}$$

$$\bar{\tau}_{R\psi}(\psi) = -\frac{\Delta P}{T}\frac{dL}{d\psi}. \quad \text{(B28)}$$

Finally, with respect to the application of Eqs. B21–B28 we make the following suggestion. For an evaluation of L and $dL/d\psi$ the expressions first introduced in Eqs. B7 and B8 should be used; namely,

$$L(\psi) = x(\psi)\sin\psi + y(\psi)\cos\psi \quad \text{(B29)}$$

$$\frac{dL(\psi)}{d\psi} = x(\psi)\cos\psi - y(\psi)\sin\psi. \quad \text{(B30)}$$

That is, there is no point in numerically differentiating a table of values of L when a closed form expression is available.

APPENDIX C

An approximation for stress difference

If we assume that stress normal to the interior surface of the cylinder varies linearly between its two extreme values at the inner and outer surfaces of the cylinder (refer to the conditions specified by Eq. A3), it will have the following mathematical form:

$$\sigma_R = \frac{\Delta P}{T}(R - R_o) - P_o. \quad \text{(C1)}$$

If we define average normal stress consistent with our previous definitions of average stress,

$$\bar{\sigma}_R = \frac{1}{T}\int_{R_i}^{R_o}\sigma_R dR,$$

it follows that

$$\bar{\sigma}_R = -\frac{\Delta P}{2} - P_o. \quad \text{(C2)}$$

Subtracting Eq. C2 from B21, B23, B25, and B27, respectively, we obtain the following results. For a single plane of symmetry,

$$\bar{\sigma}_\psi(\psi) - \bar{\sigma}_R(\psi) \approx \left[\bar{\sigma}_\psi(0) + P_o - \frac{\Delta P y(0)}{T}\right]\cos\psi + \frac{\Delta P}{T}\left(L + \frac{T}{2}\right) \quad \text{(C3)}$$

$$= -\left[\bar{\sigma}_\psi(\pi) + P_o - \Delta P\frac{|y(\pi)|}{T}\right]\cos\psi + \frac{\Delta P}{T}\left(L + \frac{T}{2}\right) \quad \text{(C4)}$$

$$= \left\{\frac{\bar{\sigma}_\psi(0) - \bar{\sigma}_\psi(\pi)}{2} - \frac{\Delta P}{T}\frac{[y(0) - |y(\pi)|]}{2}\right\}\cos\psi + \frac{\Delta P}{T}\left(L + \frac{T}{2}\right). \quad \text{(C5)}$$

For two planes of symmetry,

$$\bar{\sigma}_\psi(\psi) - \bar{\sigma}_R(\psi) \approx \frac{\Delta P}{T}\left(L + \frac{T}{2}\right). \quad \text{(C6)}$$

The authors acknowledge the expert assistance of Roshan Freeman of the Aerospace Corporation, El Segundo, CA in the preparation of this manuscript.

The authors are also grateful to the California State University Long Beach for the use of their computer facilities in conducting this research.

Received for publication 4 February 1988 and in final form 9 June 1988.

REFERENCES

1. Arts, T., R. S. Reneman, and P. C. Veenstra. 1979. A model of the mechanics of the left ventricle. *Ann. Biomed. Eng.* 7:299–318.
2. Demer, L. L., and F. C. P. Yin. 1983. Passive biaxial mechanical properties of isolated canine myocardium. *J. Physiol. (Lond.).* 339:615–630.
3. Depace, N. L., J. F. Ren, A. S. Iskandrian, M. N. Kotler, A. H. Hakki, and B. L. Segal. 1983. Correlation of echocardiographic

wall stress and left ventricular pressure and function in aortic stenosis. *Circulation.* 67:854–859.

4. Douglas, P. S., and N. Reichek. 1986. Estimation of wall stress and left ventricular mass by noninvasive techniques and clinical applications. *In* Cardiac Imaging: New Technologies and Clinical Applications. M. N. Kotler and R. M. Steiner, editors. F. A. Davis Co., Philadelphia. 103–128.
5. Heethaar, R. M., R. A. Robb, Y. C. Pao, and E. L. Ritman. 1976. Three-dimensional stress and strain analysis in the intact heart. In Proceedings of the San Diego Biomedical Symposium. J. I. Martin, editor. Academic Press, Inc., New York. 15:337–342.
6. Huisman, R. M., P. Sipkema, N. Westerhof, and G. Elzinga. 1980. Comparison of models used to calculate left ventricular wall force. *Med. Biol. Eng. Comput.* 18:133–144.
7. Jan, K. M. 1985. Distribution of myocardial stress and its influence on coronary blood flow. *J. Biomech.* 18:815–820.
8. Janz, R. F. 1982. Estimation of local myocardial stress. *Am. J. Physiol.* 242:H875–H881.
9. Janz, R. F., and R. J. Waldron. 1976. Some implications of a constant fiber stress hypothesis in the diastolic left ventricle. *Bull. Math. Biol.* 38:401–413.
10. Janz, R. F., and R. J. Waldron. 1978. Predicted effect of chronic apical aneurysms on the passive stiffness of the human left ventricle. *Circ. Res.* 42:255–263.
11. McPherson, D. D., D. J. Skorton, S. Kodiyalam, L. Petree, M. P. Noel, R. Kieso, R. E. Kerber, S. M. Collins, and K. B. Chandran. 1987. Finite element analysis of myocardial diastolic function using three-dimensional echocardiographic reconstructions: application of a new method for study of acute ischemia in dogs. *Circ. Res.* 60:674–682.
12. Mirsky, I. 1979. Elastic properties of the myocardium: A quantitative approach with physiological and clinical applications. *Handb. Physiol.* (Sect. 2, Cardiovasc. Syst., pt. I, Heart) 497–531.
13. Mirsky, I., J. N. Pfeffer, M. A. Pfeffer, and E. Braunwald. 1983. The contractile state as the major determinant in the evolution of left ventricular dysfunction in the spontaneously hypertensive rat. *Circ. Res.* 53:767–778.
14. Pouleur, H., M. F. Rousseau, C. van Eyll, and A. A. Charlier. 1984. Assessment of regional left ventricular relaxation in patients with coronary artery disease: importance of geometric factors and changes in wall thickness. *Circulation.* 69:696–702.
15. Robb, R. A. 1985. Three-Dimensional Biomedical Imaging. Volumes I and II. CRC Press, Inc., Boca Raton, FL.
16. St. John Sutton, M. G., T. A. Plappert, J. W. Hirshfeld, and N. Reichek. 1984. Assessment of left ventricular mechanics in patients with asymptomatic aortic regurgitation: a two-dimensional echocardiographic study. *Circulation.* 69:259–268.
17. Streeter, D. D., Jr., H. M. Spotnitz, D. P. Patel, J. Ross Jr., and E. H. Sonnenblick. 1969. Fiber orientation in the canine left ventricle during diastole and systole. *Circ. Res.* 24:339–347.
18. Streeter, D. D., Jr., R. N. Vaishnav, D. J. Patel, H. M. Spotnitz, J. Ross, Jr., and E. H. Sonnenblick. 1970. Stress distribution in the canine left ventricle during diastole and systole. *Biophys. J.* 10:345–363.
19. Tozeren, A. 1983. Static analysis of the left ventricle. *J. Biomech. Eng.* 105:39–46.
20. Waldman, L. K., Y. C. Fung, and J. W. Covell. 1985. Transmural myocardial deformation in the canine left ventricle. *Circ. Res.* 57:152–163.
21. Yin, F. C. P. 1981. Ventricular wall stress. *Circ. Res.* 49:829–842.
22. Yin, F. C. P., P. H. Chew, and S. L. Zeger. 1986. An approach to quantification of biaxial tissue stress-strain data. *J. Biomech.* 19:27–37.
23. Zile, M. R., W. H. Gaasch, J. D. Carroll, and H. J. Levine. 1984. Chronic mitral regurgitation: predictive value of preoperative echocardiographic indexes of left ventricular function and wall stress. *J. Am. Coll. Cardiol.* 3:235–242.